Enhanced selectivity in mixed matrix membranes for CO_2 capture through efficient dispersion of amine-functionalised MOF nanoparticles.

Behnam Ghalei, [a] Kento Sakurai, [ab] Yosuke Kinoshita, [ab] Kazuki Wakimoto, [ab] Ali Pournaghshband Isfahani, [a] Qilei Song, [c] Kazuki Doitomi, [d,e] Shuhei Furukawa, [a] Hajime Hirao, [d,e] Hiromu Kusuda, [b] Susumu Kitagawa [a] and Easan Sivaniah [a] *

a. Institute for Integrated Cell-Material Sciences (iCeMS), Kyoto University, 606-8501 Kyoto, Japan.

b. Department of Energy Science and Technology, Kyoto University, Kyoto, Japan.

c. Department of Chemical Engineering, Imperial College, London, SW7 2AZ, UK.

d. Department of Biology and Chemistry, City University of Hong Kong, Tat Chee Avenue, Kowloon, Hong Kong, China

e. Division of Chemistry and Biological Chemistry, School of Physical and Mathematical Sciences, Nanyang Technological University, 21 Nanyang Link, Singapore 637371

*Correspondence and requests for materials should be addressed to E.S. Email: esivaniah@icems.kyoto-u.ac.jp

Mixed Matrix Membranes (MMMs) for gas separation applications, have enhanced selectivity when compared with the pure polymer matrix, but are commonly reported with low intrinsic permeability, which has major cost implications for implementation of membrane technologies in large scale carbon capture projects. High permeability polymers rarely generate sufficient selectivity for energy efficient CO_2 capture. Here we report substantial selectivity enhancements within high permeability polymers as result of the efficient dispersion of amine-functionalized, nanosized MOF additives. The enhancement effects under optimal mixing conditions occur with minimal loss in overall permeability. Nanosizing of the MOF enhances its dispersion within the polymer matrix to minimize non-selective microvoid formation around the particles. Amination of such MOFs increases its interaction to the polymer matrix, resulting in a measured rigidification and enhanced selectivity of the overall composite. The optimal MOF MMM performance was verified in three different polymer systems, and also over pressure and temperature ranges suitable for carbon capture.

The current default technology for large scale CO_2 capture and storage (CCS) is based on liquid phase absorption towers; whilst many projects of this sort are proposed, few reach completion as costs become prohibitive[3]. Therefore, it is imperative to offer more cost-effective technological solutions. Membrane separation is often considered; however, current commercial membrane technologies are virtually as expensive as adsorption technologies. This is because gas fluxes through selective membranes are so low that hundreds of millions of m^2 of commercial membranes are required even for a single 1000MW power station[5]. When combined with membrane costs of ~\$50/m^2, the capital cost for commercial membrane based solutions to CCS is not that different from the unpalatably high costs of adsorption towers for CCS. The key to a future membrane based

CCS solution lies in significantly reducing the total membrane areas required, which in turn requires cheap, higher permeability membrane materials that retain a high selectivity. New research is aimed at developing better performance polymers (in selectivity and permeability); however the timelines for reducing costs of such polymers may not be compatible with needs to find immediate candidate materials for large scale membrane based CCS solutions.

Typically, commercial membrane materials have low permeability of a few tens of Barrers (1 Barrer = 10^{-10} cm^3 (STP) cm cm^{-2} s^{-1} $cmHg^{-1}$), but have acceptable selectivity for CO_2 removal from flue-stack or natural gas sources. Merkel and co-workers [5] have shown it is imperative to generate materials with orders-of-magnitude enhanced permeability whilst maintaining such selectivity, to cost-effectively process the massive volumes of flue gas in power plants. Microporous materials used for membrane technology potentially include inorganic and organic frameworks, such as zeolites[7], metal-organic frameworks (MOFs)[8] and covalent organic frameworks[9]. However, commercial membranes units contain thin films of the selective material where practical processability and physical durability requirements tend to favor the use of tough polymeric thin films. Gas transport in most polymers can be explained with the solution diffusion model, where the permeability coefficient (*P*) is a product of solubility (*S*) and diffusion coefficient (*D*)[10]. Polymers of Intrinsic Microporosity (PIMs)[11,12], are a sub-class of microporous polymers with a rigid, contorted backbone structure (for example, PIM-1 in Figure 1) and high intrinsic permeabilities (e.g. P_{CO2} ~ 3000 Barrer), but with low selectivity compared to commercial polymers (30-50 for CO_2/N_2 separations)[13]. Thermal and other post-processing of PIM-1 and other polymers such as TR-polymers[14] leads to enhanced permeability-selectivity performance[14-17]. However, thermal processing (often at temperatures not compatible with the rest of the membrane support structure) adds complexity to the final technology.

Figure 1. Fabrication of MMMs in this study. (a) UiO-66 synthesised from zirconium ion and terephtalic acid, (b) Reducing the UiO-66 size using water modulation and functionalization of the MOF walls, (c) Molecular structure of PIM-1 and (d) Combination of PIM-1 and MOF particles to form MMMs. Carbon atoms are depicted as green; oxygen and hydrogen atoms are in red and white, respectively; Nitrogen, NH_2 and bromine are presented in blue.

A simpler approach than post-treatment of polymer membranes, or cheaper than the synthesis of a high-performance speciality polymer, is through mixed matrix membranes (MMMs); this is the concept of combining the attractive properties of polymeric and inorganic microporous materials[18]. Initially this has been through the addition of zeolites, silicas or activated carbons but recently, focus has shifted towards the addition of MOFs to the polymer matrix[19,20]. The tightly regulated pore structures of MOFs, and the chemical interaction with the matrix can be fine-tuned by selecting appropriate organic ligands; a feature which is less available to other fillers [21]. In this study we generate MMMs that have both high selectivity and permeability through the combination of PIM-1 polymers and a Zr-based MOF system, UiO-66, known for its chemical and thermal stability (Figure 1) [22]. Since PIM-1 is already a high permeability material, we seek to enhance its selectivity through the addition of UiO-66. Usually, the addition of a MOF to a polymer matrix increases the overall permeability of the material but does little for its selectivity. Here, we show that a reduction in MOF size, through water modulated synthesis[23], has a divergent effect of enhancing gas pair selectivity noticeably without affecting permeability. Also, we alter the MOF's functionality; a combination of these two parameters leads synergistically to similarly enhanced membrane selectivity in three, commercially used polymer membrane matrices.

Figure 2. MOF and MMM physical characterization. SEM images of dried aggregates of (a) microsized UiO-66-ref and (b) water modulated nanosized UiO-66-H MOF nanoparticles (scale bars: 200 nm). (c) PXRD analysis of PIM-1 membranes with different UiO-66-NH_2 loadings. SEM images of cross-sections of PIM-1/UiO-66 MMMs containing (d)-(f) 20 wt.% UiO-66-ref and (g)-(i) 20 wt.% water modulated UiO-66-NH_2 with different magnifications. Photos of MMM containing (j) 20 wt.% UiO-66-ref and (k) 20 wt.% water modulated UiO-66-NH_2.

Polymer and MOF synthesis and characterization. PIM-1 was synthesized from a polycondensation reaction between 5,5',6,6'-tetrahydroxy-3,3,3',3'-tetramethyl-1,1'-spirobisindane and 1,4-dicyanotetrafluorobenzene crystals (Supplementary Figure 1) [24]. Zr-MOFs were prepared using zirconium tetrachloride ($ZrCl_4$) and three different organic ligands (terephthalic acid, 2-amino-1,4-dicarboxybenzene and 2-bromo-1,4-dicarboxybenzene); Water modulation was used to make nano-sized UiO-66 particles (Supplementary Figures 2 and 3) [25]. For clarity, the reference system in this study is UiO-66-ref, a non-water modulated Zr-MOF having simple terephthalic acid

linkers. All other Zr-MOFs, produced via water modulation, are termed UiO-66-H, UiO-66-NH_2 or UiO-66-Br in reference to the additional functionality on the ligand.

UiO-66-ref particles showed agglomerated cubic crystals of around 100-200 nm (Figure 2(a)). After water modulation, the particle morphology changed towards smaller (20-30 nm) nanocrystals in UiO-66-H (Figure 2(b)), UiO-66-Br and UiO-66-NH_2 particles (Supplementary Figure 5). N_2 sorption isotherms of all UiO-66 powders indicated the presence of microporosity (with the pore size being less than 2 nm) owing to the framework structure, and mesoporosity (2-50 nm) arose from interstitial voids between aggregated nanoparticles (Supplementary Figure 6).

The BET surface area of water modulated UiO-66-H is 1115.4 $m^2 g^{-1}$, which is a little lower than that of the larger UiO-66-ref particles (1320 $m^2 g^{-1}$). In the functionalized UiO-66-NH_2 and UiO-66-Br, the BET surface areas decreased to 708.6 and 585.4 $m^2 g^{-1}$, respectively. This is attributed to protrusions of the bulky $–NH_2$ or –Br groups into the empty space of the micropores [26] (Supplementary Table 1). The correlation between BET areas, crystallinity and modulation are complicated by modulated small particles having more internal defects (lower crystallinity) as well as void spaces within MOF aggregates. An extended discussion of such factors is in Supplementary Note 1.

Zr-MOFs with different functionalities and particle size were dispersed into a PIM-1 solution in different loadings of 5 to 40 wt.% and used to prepare ~80 μm thick polymer membranes. The degree of loading and chemical signature of the additives was additionally confirmed from FTIR and TGA analysis (Supplementary Figures 3, 4, 7 and 8) whilst PXRD analysis of the composites confirmed the integrity of the MOF nanocrystals at any loading of particles into the matrix (Figure 2(c)).

Figure 3. Computational studies of adhesions between PIM-1 and UiO-66 particles. (a) Models of the UiO-66 and UiO-66-NH_2 frameworks. UiO-66-A and UiO-66-NH_2-A feature corrugated surfaces, while UiO-66-NH_2-B have a flat surface. Target sites for PIM-1 sampling are shown in stick representation. (b) The highest-ranked structures of the UiO-66-A/PIM-1 composite (UiO-66-A-1). (c) The highest-ranked structures of the UiO-66-NH_2-A/PIM-1 composite (UiO-66-NH_2-A-1). The MOF and PIM-1 are shown in stick and ball-and-stick representations, respectively, in (b) and (c). Carbon atoms depicted as purple balls and green sticks in PIM-1 and UiO-66 MOFs, respectively; nitrogen atoms are presented in blue. Oxygen and hydrogen atoms are in red and white, respectively. Interatomic distances are presented in Å. USCF Chimera was used for visualizing molecular structures.

The differences in optical transparency (see Figures 2(j) and (k)) between micro- and nano-MOF MMMs confirm the improved dispersion of the modulated Zr-MOF. Large agglomerates (Figure 2(d)-(f)) are seen in cross-sectional electron microscopy (SEM) of the un-modulated MOF MMMs; these are not observed for the case of the modulated UiO-66-NH_2 based MMMs (Figure 2(g)-(i)). The particle/polymer interfacial adhesion was also improved markedly when particles contained -NH_2 groups (Supplementary Figure 9).

Computational studies. To gain insight into the adhesion processes between PIM-1 and UiO-66 MOFs, a series of simulations were conducted using the Adsorption Locator and Forcite programs in Material Studio. PIM-1, UiO-66 and UiO-66-NH_2 were described using the universal force field (UFF)[27] and QEq charges [28]. Using the crystal structure of UiO-66, two types (A and B) of models for UiO-66 and UiO-66-NH_2 were built (Figure 3(a)) [29]. UiO-66-A and UiO-66-NH_2-A feature non-flat, corrugated surfaces, while UiO-66-B and UiO-66-NH_2-B have flat surfaces. The total charge is zero in all cases. In a separate simulation, the stability of corrugated UiO-66 surfaces was found to be higher than that of the flat surfaces (Supplementary Note 2). The simulations of MOF-PIM-1 interactions yields several plausible adhesion geometries, and we analyzed the top three geometries that exhibited large adhesion energies. The largest negative adhesion energy of UiO-66-NH_2-A-1 (-72.2 kcal/mol) is significantly larger in magnitude than that of UiO-66-A-1 (-55.3 kcal/mol) (Supplementary Note 2 and Supplementary Table 2). It should be noted that these simulations involve oligomers of the PIM-1 monomer. However, such polymeric-MOF simulations[30] do more rigorously confirm the tentative finding here that enhanced MOF/PIM-1 interfacial adhesion in the case of UiO-66-NH_2 should be primarily due to the H-bonding interactions at the corrugated surface.

Gas transport properties. As the large UiO-66-ref particles loading increases up to 10 wt.%, all the single gas permeabilities increased dramatically whilst the ideal selectivity remained similar to that of the pure polymer (Figure 4(a), (b) and Supplementary Table 4 and Supplementary Figure 13). At higher loading, i.e. 20 wt.%, the permeability increased to around two times that of the pure polymer; this higher permeability and lower selectivity is a conventional behaviour and can be attributed to the non-selective diffusion at a defective interface between MOF particle and polymer, as observed in the SEM showing 'Sieve-in-a-cage' morphology [31].

In sharp contrast, at low loadings of modulated UiO-66, a minimal change in CO_2 permeability, and an increase in ideal selectivity was observed (Supplementary Table 4). At higher UiO-66 loadings, the permeability decreased, in contrast to the larger UiO-66-ref fillers, whilst the general selectivity of the gases remains at a higher plateau.

This trend of an enhanced selectivity was greatly improved for MMMs containing amine functionalized, *and* size modulated MOFs, UiO-66-NH_2, with the optimal conditions for selectivity and permeability seen at low loadings (5-10 wt%) (Figure 4(a) and (b)). By contrast, the introduction of the bromo-functionalized UiO-66 particles into the PIM-1 membrane does not alter the selectivity significantly in the separation (Supplementary Table 4). There is a decrease in the membrane permeability as more modulated filler is added to the system. This is attributed to the collection of the smaller modulated fillers into an essentially non-porous aggregate. In fact as Figure 3(a) and (b) show, as the total filler content approaches 40%, there are deviations in the trends of permeability and selectivity that may indicate some connectivity of these aggregated phases at high contents, whose structure-property relationship is more difficult to interpret.

The results reported here (including mixed gas and high pressure in Supplementary Figures 16 and 17) are

Figure 4. Gas transport properties. (a) Gas permeability (green diamond: CO_2, blue triangle: O_2, purple triangle: CH_4 and red circle: N_2**)** and (b) Ideal selectivity (black square: CO_2/CH_4, red circle: CO_2/N_2 and blue diamond: O_2/N_2) in MMMs as a function of smaller amine functionalized UiO-66-NH_2 (closed symbols) or larger un-functionalized UiO-66-ref loadings (open symbols) at 298 K and 4 bar. The average permeation data is presented; error bars represent the standard error of three membranes (n=3). (c) A direct comparison of PIM-1/MOF CO_2/N_2 selectivity enhancement for reported data for PIM-1 based MMMs; right half-filled squares: 1, 2, 3 [1], 4 [2] and 5, 6 [4]; are compared to 5 and 10 wt% filler loadings of UiO-66-NH_2 (red circle), UiO-66-Br (blue circle) UiO-66-H (green circle) and UiO-66-ref (purple circle). (d) A Robeson plot of ideal CO_2/N_2 selectivity provides a recent review of MOF MMMs (black squares refer to enhancements over the pure polymer in selectivity and permeablity: upper half-filled and right half-filled squares refer to only selectivity or permeability enhancements respectively) in comparison to UiO-66-NH_2 and UiO-66-ref based MMMs with different filler loadings (presented as wt%); red and purple arrows show the enhancements in CO_2/N_2 ideal selectivity and CO_2 permeability compare with PIM-1 (black open circle) by adding UiO-66-NH_2 and UiO-66-ref, respectively. The region for target performance of membranes for CO_2 capture from flue gas inferred from Merkel et al. [5] is shown by the blue box; blue line shows the empirical Robeson upper bound for properties of state-of-the-art polymer membranes as summarized in reference [6] in 2008.

compelling in generating a high permeability membrane with comparatively large selectivity enhancements which range from ~70% for CO_2/N_2 separation, to ~95% for CO_2/CH_4 separation (Figure 4(a) and (b)). The upper bound plot shows that the gas permeability of PIM-1 composites containing UiO-66-NH_2 nanoparticles is enhanced over the basic selectivity of PIM-1 and sits within a recently reported selectivity/permeability window required for the optimum CO_2 separation performance of membranes from the flue gas (See Figure 4(d)).

To be precise, the window is defined by Merkel *et al.* [5] for membranes having permeance greater than 1000 gas permeation units, (GPU) and CO_2/N_2 selectivity of at least 20, with consideration of the overall cost of carbon capture using membrane processes and inclusive of plant operating costs and capital costs so as to compare membrane capture costs to current capture costs via amine scrubbing processes (~$40-100/Tonne CO_2). Since we later demonstrate a practical 1 μm CCS capable membrane in this paper, we use this thickness to convert permeance to permeability though it should be noted that thinner (100-200 nm) membranes are technically possible.

It is very revealing to specifically compare our data to other recently reported PIM-1/MOF studies since a focus of this research is to create MMMs that enhance selectivity of the highly permeable PIM-1. Shown in Figure 3(c) are three currently reported PIM-1 based MOF-MMMs, using UiO-66, titanium exchanged UiO-66, UiO66-NH_2 and also ZIF-8. The data is normalized against those laboratory's own values for pure PIM-1 behaviour. The trend of such data is self-

similar indicating that UiO-66 addition leads to enhanced permeability but little relative improvement in selectivity.

The difference between our reported data and those, non-modulated UiO-66 MOF fillers is striking. Using water modulation in our studies to generate small MOF particles leads to enhanced selectivity at little loss in permeability. Moreover, this selectivity enhancement is accentuated by the use of MOF surface functionality with -NH_2 groups. The enhanced performances reported here can be rationalized by recognizing the importance of size, functionality and loading-induced phase behavior in optimizing the generation of high performance mixed matrix gas separation membranes [31]. Several of the higher performance results show that the better selectivity enhancements are seen at relative low MOF additions of 5-10 wt.%, suggesting that aggregation at higher loadings reduces the effectiveness of additional filler loading [21].

At low loadings (up to 10 wt%) of modulated UiO-66-H particles the selectivity enhancement is intermediate to what can be attained with additional amine functionality. The additional selectivity is unlikely to arise from the aminated MOF's adsorption selectivity contribution given that the enhanced selectivity is optimized at low loadings. A more reasonable explanation is that the highly dispersed amine-functionalized surfaces have altered the distribution of porosity and rigidity in the surrounding polymer matrix; this is a well-known principle [32-34] that arises from a strong interaction between the polymer and the solid surface. A closer comparison of the FTIR spectra for PIM-1 composites containing UiO-66-ref or UiO-66-NH_2 indicate differences in ether stretching bond absorption that support the idea of an interactive MOF-polymer interface in UiO-66-NH_2 composites (Supplementary Figure 7). Rigidification of the polymer leads to increased selectivity, but also leads to low permeability. However, for low MOF additions, there is a selectivity increase but no loss in overall permeability since the UiO-66 MOF itself is a large pore system that compensates for the loss in PIM-1 permeability in the composite.

It is important to emphasize that Figure 4(d) only includes high permeability MMM data (CO_2 permeability >100 Barrer) using MOF fillers. It does not intend to engage in a broader

196 comparison to the properties of emerging pure polymers reported in the literature since the premise
197 of this work is the value and simplicity of adding a MOF filler to an established polymer system.
198 For the case of other MOF data, the square symbols (upper half-filled, right half-filled and filled)
199 indicate where the MOF addition has respectively increased selectivity, permeability or both. The
200 clear conclusion is that MMMs using MOFs tend to increase permeability, and significant
201 enhancements in selectivity are rarely observed.

202 Various trends of MMMs in terms of relative trade-offs in permeability and selectivity have
203 recently noted [2]. Many selectivity enhancements are seen with the addition of activated carbons or
204 fused silica fillers[35]. The significant account of the various reported combinations of MOF
205 MMMs[19,20] was used to generate the comparative results in Figures 4. Additionally it has shown
206 that amine-functional groups in synthesized MOF-199 increased the CO_2/CH_4 selectivity (up to
207 35%) in 6FDA–ODA polyimide MMMs[36]. Another study also reported ~50% selectivity
208 enhancement in CO_2/CH_4 separation through the use of benzoic acid modulated amine
209 functionalized UiO-66 particles, albeit with a single and high loading (30 wt%) and a low-

Figure 5. Mechanical studies of PIM-1 MMMs and demonstration of similar performance in other polymer MMMs. (a) Young's modulus and indentation hardness of PIM-1/UiO-66 MMMs at different loadings; Error bars represent the standard error of 20 indents (n=20). The measurements were performed at ambient temperature. The average values of the elastic modulus (E) and the hardness (H) were calculated in the depth of 4 μm. (b) Aging behaviour of PIM-1 (open symbols) and PIM-1/UiO-66-NH_2 (10 wt% filler) MMMs (closed symbols); N_2 permeability (green triangles), CO_2 permeability (red circles) and CO_2/N_2 selectivity (blue square). All measurements conducted at 4 bar and 25 ˚C. Samples were kept under vacuum condition at 25 ˚C in between measurements for the aging study (c) Cross section SEM of PIM-1/UiO-66-NH_2 thin film membrane on the surface of a ceramic support with 5 wt.% filler, scale bar is 500nm. (d) CO_2/N_2 selectivity of UiO-66-NH_2 MMMs within different polymers, grey: PIM-1, red: Pebax® and blue: polyurethane. The number on each column represents the CO_2 permeability (Barrer) of corresponding membranes.

210 permeability polyimide matrix[37]. Adding MOF nanosheets lead to increase in selectivity by 35%,
211 again over the base matrix of polyimide[38]. As is apparent in the recent review of MOF-based
212 MMMs[20], these enhancements in selectivity are predominantly reported for MMMs (such as
213 6FDA–ODA, Matrimid or Pebax®) with permeabilities that are 1-2 orders of magnitude lower than
214 what are possible with PIM class materials.

215 Therefore, it is also instructive to frame our data within a more complete survey of MOF-
216 Polymer results (as compiled in the literature survey in Supplementary Tables 6-10). It can be

concluded that while significant enhancements are seen for MOF additions to very low permeability polymers (CO_2 permeability <100 Barrer), the data presented here represents a similar level of selectivity enhancement achieved in polymers of high permeability (CO_2 permeability >1000 barrer).

Mechanical effects of microscopic rigidification. Young's Modulus and hardness values of the membrane containing the larger UiO-66-ref fillers or the amine-functionalized, water modulated UiO-66-NH_2 were determined (Figure 5(a) and Supplementary Figure 18). It was found, for the UiO-66-ref composites, that the mechanical properties were reduced with respect to the basic polymer properties.

However, in the case of UiO-66-NH_2, the mechanical properties were actually enhanced for low MOF compositions, corresponding to the optimal MOF gas separation performance (5-10 wt%). At higher MOF compositions, the mechanical properties deteriorated again, as might be expected when there is more aggregation of the MOF additives within the system. Notably, loadings of up to 20 wt% of UiO-66-ref were possible before the membrane composite became too fragile to handle for gas separation studies; twice as much loading was possible using nanosized UiO-66-H, UiO-66-NH_2 and UiO-66-Br. Such observations corroborate the mechanical test findings.

Aging is the phenomenon where glassy materials, over a protracted time, relax to a denser configuration [39]. Therefore, PIM-1 by itself, with a large initial free volume due to the poor packing of an irregular backbone, has a well-known initial loss in permeability over a month [40,41], but gains in selectivity. The addition of the amine-functionalized, water modulated UiO-66-NH_2 MOF additive to PIM-1 was found to stabilize this long time again behaviour, leading a more consistent selectivity performance over a one year aging study period (Figure 5(b)).

Practical membranes are generated using a thin film of the membrane (for spiral wound gas modules). In such instances, the bulk permeability and selectivity can be a poor indicator of the final material performance since thin film processing conditions do not match the slowly equilibrated bulk material studies [42]. For example, 1μm thick PIM-1 films were prepared on a

ceramic support; its CO_2/N_2 selectivity, at 9, loses 45% of its bulk selectivity (Figure 5(c)). The enhanced mechanical properties in the UiO-66-NH_2 MMM might be expected to enhance its thin film stability. Thus it is found that the addition of the amine-functionalized, water modulated UiO-66-NH_2 allows the one micron thick MMM films to retain nearly 90% of its bulk CO_2/N_2 separation power (see Table 1 and Supplementary Figure 20).

Table 1. Gas separation performance of thin film membranes at 1 bar and 25 ℃.

Membrane	Permeance (GPU)		Ideal selectivity
	N_2	CO_2	CO_2/N_2
PIM-1	390	3600	9.2
5 wt% UiO-66-NH_2	72	1740	24.1

Whilst PIM-1 is an attractive future membrane separation material, especially for CCS, the same selectivity enhancement (with low permeability loss) using these water modulated aminated fillers can be achieved in commercially used polymers as Pebax® or polyurethane. This is demonstrated in Figure 5(d), where the same optimal enhancement of CO_2/N_2 selectivity of ~70% is observed for all three materials. It is notable that whereas PIM-1 is a glassy polymer, the polyurethane is a rubbery material, and one finds an optimal selectivity enhancement using higher loadings of the amine-functionalized, water modulated UiO-66-NH_2 MOF additive.

Conclusions. Commercial polymer membranes can have high absolute selectivity values. However a significant problem is that the permeability of commercial membranes is limited leading to large operation and capital costs, especially when considering the enormous volumes of flue-gas emitted from a single power station. Achieving satisfactory selectivity in high permeability membranes will lead to a significant reduction in the membrane area required. Microporous materials, such as PIM-1 have exceptionally high permeability but a low CO_2/N_2 selectivity which makes separation efficiency low. This paper demonstrates that the addition of a MOF (properly sized and functionalized) has the ability to significantly enhance the selectivity of a high permeability microporous material. The attractiveness of a mixed matrix approach for gas separation membranes is to generate superior performances by the simple combination of the attractive features of its

polymeric and inorganic components. Nonetheless a commonly observed trend is an increase in membrane permeability and loss of selectivity upon addition of a MOF filler. In this paper, we observe the divergent trend of enhanced selectivity and minimal permeability losses. This effect is achieved primarily through minimization of the MOF fillers size during it synthesis via water modulation techniques. The effect is further enhanced by tuning the MOF surface functionality. The resulting MOF MMMs had corollary improvements in its overall material mechanical properties. Due to their amenability to such tuning, metal organic frameworks, used in this fashion, are an accommodating class of filler for achieving high performance gas separation membranes through the mixed matrix membrane concept. The particular polymer/MOF combination demonstrated here may not be the final solution, but the approach may be optimized and is a significant tool towards preparation of membranes for economical CO_2 capture.

Methods

Synthesis of polymer. PIM-1 was synthesized from polycondensation reaction between 10.2 g purified 5,5',6,6'-tetrahydroxy-3,3,3',3'-tetramethyl-1,1'-spirobisindane (TTSBI, Sigma-Aldrich) and 6g purified 1,4-dicyanotetrafluorobenzene crystal (DCTB, Wako Pure Chemical) in the presence of 8.3 g dried K_2CO_3 (Sigma-Aldrich) and 200 ml anhydrous dimethylformamide (DMF, Wako Pure Chemical). The mixture solution was stirred under nitrogen atmosphere at 65 °C for 60 h. The solution was then cooled and poured into 500 mL of pure water. The solid precipitated polymer was then purified by dissolving in chloroform and re-precipitation from methanol, filtered and dried in vacuum oven at 110°C overnight [24]. The molecular weight of purified polymer was determined from gel permeation chromatography (GPC), giving an average molecular weight of *Mn* = 110,000 Dalton and a polydispersity (PDI) of 2.1. Polyurethane was synthesized by a two-step bulk polymerization method. Pluronic L35 was reacted with an excess IPDI (PTMG:IPDI 1:3 molar ratio) under nitrogen atmosphere at 75°C to obtain a macro diisocyanate pre-polymer. After 2h, chain extender (1,8-octanediamine) with molar ratio of PTMG: IPDI: chain extender (1:3:2) was added to the reaction. The synthesized PU washed and precipitated in methanol: water (50:50 wt%) to remove any unreacted monomers or low molecular weight polymers. Samples dried at 80°C under vacuum before using. The gel permeation chromatography (GPC) was used to determine molecular weight of the synthesized PUs, giving an average molecular weight of *Mn* = 85,400 Dalton and a PDI of 2.2.

Synthesis of UiO-66 derivatives. Various derivatives of UiO-66 particles (Zr-MOFs) were prepared from a mixture of zirconium tetra chloride ($ZrCl_4$), different organic ligands including terephthalic acid (UiO-66), 2-amino-1, 4-dicalboxybenzene (UiO-66-NH_2), 2-bromo-1, 4-dicalboxybenzene (UiO-66-Br), and dimethylformamid (DMF) in the 2.3 mmol: 2.3 mmol: 30 mL ratio. After 30 min stirring, the slurry was introduced in a 100 mL teflon-lined autoclave and heated at 120 ˚C for 24 h. The resulting UiO-66 crystals were separated by centrifugation, followed by washing with methanol twice to remove the excess of unreacted ligand. The final powder was washed with chloroform over 3 days, exchanging the chloroform each day and finally dispersing as colloids in fresh chloroform for use in membrane preparation. In order to decrease the crystal size and making nano-sized UiO-66 particles, 113.5 mmol of water is slowly added to the slurry reaction solution, including zirconium tetra chloride, organic ligand and DMF, and stirred for 10 min before heating up to 120 ˚C [22]. As control samples, one batch of UiO-66 particles was dried under vacuum at 150 ˚C for 12 h and stored dry for further analysis. The yield of UiO-66 particles was about 45 mol% based on the ideal molar conversion of zirconium.

Zr-MOFs based MMMs. The known concentration of as-synthesized Zr-MOF colloidal solution (UiO-66, UiO-66-Br and UiO-66-NH_2) in chloroform was sonicated to prevent particulate aggregation. The dried PIM-1 dissolved in chloroform (8 wt.%) and then filtered through the PTFE syringe filter (0.45 µm) into the particle suspension solution. The resulting PIM-1-filler solution was stirred overnight. After sonication to remove the air bubbles, the resulting PIM-1/Zr-MOF solutions were cast onto a clean glass substrate, covered and placed in a glove bag. The membranes were allowed to form at ambient temperature by solvent evaporation over two days. The membranes were removed from the

glass substrate and dried at 110 ˚C under vacuum prior to gas permeation and structure characterization. Nanocomposite membranes were prepared with loadings of Ui-O66 based particles at 5, 10, 20, 30, and 40 wt%. The thickness of the final pure and composite membranes varied within the range of 80-100 μm, depending on the loading of Zr based particles as measured by a micrometer (Mitutoyo, Model S406, Japan). Thin film samples have been prepared by spin coating of 4 wt% solution containing PIM-1 and UiO-66-NH_2 particles in chloroform on the surface of Anodisc® flat disc membranes. Pebax® 2533 (Arkema Co.) and polyurethane samples casted from 8 wt% polymer solution with and without MOF particles in N-Methyl-2-pyrrolidone (NMP).

Characterization. The obtained functional groups in synthesized PIM-1 and Zr-based particles were investigated by the Fourier Transform Infrared spectrometer (FT-IR, Shimaduzo, IRTracer-100), equipped with an attenuated total reflectance (ATR) cell in the range of 4000–500 cm^{-1}. The crystalline structure of fillers in this work were characterized using a powder X-ray diffraction (PXRD, Rigaku RINT, Japan) with Cu Kα anode operated at 40 mA and 40 kV. Synthesized powders were crushed using a pestle and mortar. A small amount of sample was then mounted onto the sample holder and flattened using a glass slide. The samples were then scanned over a 2θ range of 5-60° . Nitrogen adsorption isotherms of Zr-MOF structures was undertaken using BELSORP- Max instrument (BEL Inc. Japan) at 77 K to investigate the specific surface area and porosity of the Ui-O66 particles. The pressure was adjusted within the adsorption chamber until the inside pressure is equilibrated within the target pressure interval (less than 10 Pa difference). The equilibrium time varied between few minutes to several hours depending on the type of gas and pressure at each points. Generally, long equilibration times at low relative pressure was observed due to diffusion of gases into the micropores. Each experiment was performed over a period of approximately one day which is the common practice for these samples. The specific surface area (SBET) was calculated based on the Brunauer–Emmett–Teller (BET) model [43]. The samples were degassed at 100 °C for 24 h under vacuum (10^{-6} bar), before testing. Thermalgravimetric analysis (TGA, Rigaku TG8120, Japan) was employed under flowing nitrogen with 10 K/min ramp rate to study the degradation temperature and the actual amount of the particles in the mixed matrix membrane. The surface and cross-section morphology of the synthesized particles and composite membranes were observed by an FESEM (Hitachi S-4800, Japan) instrument. Cross-sections of membranes were obtained by fracturing in liquid nitrogen and sputtered with osmium to prevent charging. Nanomechanical characterization including Young's modulus (E) and indentation hardness (H) were performed using nanoindentation tester (ENT 2100, Elionix) equipped with a Berkovich three-sided pyramid diamond tip (radius of 100 nm) with the load range of 0.01 to 50 mN. Each indent was made in the samples up to a maximum depth of around 4 μm. 20 points in a rectangular configuration were tested on each sample; the average data calculated based on the measured values of three different samples.

Gas permeation. Pure gas permeabilities of the membranes were determined using the constant pressure-variable volume method. The membrane was held in a Millipore commercial filter holder with steel meshed supports. The gas permeate pressure were recorded by pressure transmitters (Keller PAA 33X) connected to a data acquisition system. The slope of pressure increase (dp/dt) in the permeate chamber became constant at the pseudo-steady state. The gas permeability (P) is calculated based on the following equation:

$$P = \frac{Vl}{A}\frac{T_0}{p_f p_0 T}\left(\frac{dp}{dt}\right) \quad (1)$$

where P is the permeability of the gas through the membrane, in Barrer (1 Barrer=10^{-10} cm^3(STP)cm·cm^{-2}·s^{-1}·$cmHg^{-1}$), V is the permeate volume (cm^3), l is the thickness of membrane (cm), A is the effective area of the membrane (cm^2), p_f is the feed pressure (cm-Hg), p_0 is the pressure at standard state (76 cm-Hg), T is the absolute operating temperature (K), T_0 is the temperature at standard state (273.15 K), (dp/dt) is the slope of pressure increase in the permeate volume at pseudo-steady state (cmHg/s).

The diffusion coefficient (D) for a specific gas can be derived from the thickness of the membrane and the time lag (θ):

$$D = \frac{l^2}{6\theta} \quad (2)$$

Then the solubility (S) can be derived from:

$$S = \frac{P}{D} \quad (3)$$

The ideal selectivity ($\alpha_{A/B}$) of gas pairs, A and B, is defined as:

$$\alpha_{A/B} = \frac{P_A}{P_B} = \left[\frac{D_A}{D_B}\right]\left[\frac{S_A}{S_B}\right] \quad (4)$$

where D_A/D_B is the diffusivity selectivity and S_A/S_B is the solubility selectivity.

The feed side pressure of the gases ranged from 2 to 32 bar and operating temperature varied between 25 to 55 ˚C. For the data of each polymer membrane or polymer-MOF combination, three membrane samples were prepared and tested, and their average permeation results are presented. The error for the absolute values of the permeability coefficients could be estimated to about ±7%, due to uncertainties in determination of the gas flux and membrane thickness. However, the reproducibility was better than ±5%.

The mixed gas permeation was measured using the constant pressure-variable volume method. The membrane was exposed to CO_2/N_2, CO_2/CH_4 (50/50 vol. %, Kyoto Teisan Co., Japan) mixed gas with feed pressure up to 16 bar at room temperature (25 °C), the feed flow rate was controlled by a metering valve and measured by a flow meter (Shimadzu). The permeability and compositions of permeate gas mixtures were measured by an in-line gas chromatograph (Shimadzu, model 2014) equipped with a thermal conductivity detector (TCD) in presence of Helium as a carrier gas.

Data Availability. The data that support the findings of this study are available from the corresponding author upon request.

References

1 Khdhayyer, M. R. *et al.* Mixed matrix membranes based on UiO-66 MOFs in the polymer of intrinsic microporosity PIM-1. *Separation and Purification Technology* **173**, 304-313 (2017).

2 Bushell, A. F. *et al.* Gas permeation parameters of mixed matrix membranes based on the polymer of intrinsic microporosity PIM-1 and the zeolitic imidazolate framework ZIF-8. *Journal of Membrane Science* **427**, 48-62 (2013).

3 Reiner, D. M. Learning through a portfolio of carbon capture and storage demonstration projects. *Nature Energy* **1**, 15011 (2016).

4 Smith, S. J., Ladewig, B. P., Hill, A. J., Lau, C. H. & Hill, M. R. Post-synthetic Ti exchanged UiO-66 metal-organic frameworks that deliver exceptional gas permeability in mixed matrix membranes. *Scientific reports* **5,** 7823 (2015).

5 Merkel, T. C., Lin, H., Wei, X. & Baker, R. Power plant post-combustion carbon dioxide capture: An opportunity for membranes. *Journal of Membrane Science* **359**, 126-139, doi:http://dx.doi.org/10.1016/j.memsci.2009.10.041 (2010).

6 Robeson, L. M. The upper bound revisited. *Journal of Membrane Science* **320**, 390-400 (2008).

7 Lai, Z. *et al.* Microstructural optimization of a zeolite membrane for organic vapor separation. *Science* **300**, 456-460 (2003).

8 Kitagawa, S., Kitaura, R. & Noro, S. i. Functional porous coordination polymers. *Angewandte Chemie International Edition* **43**, 2334-2375 (2004).

9 Song, Q. *et al.* Porous Organic Cage Thin Films and Molecular-Sieving Membranes. *Adv Mater* **28**, 2629-2637, doi:10.1002/adma.201505688 (2016).

10 Freeman, B. D. Basis of Permeability/Selectivity Tradeoff Relations in Polymeric Gas Separation Membranes. *Macromolecules* **32**, 375-380, doi:10.1021/ma9814548 (1999).

11 Budd, P. M. *et al.* Polymers of intrinsic microporosity (PIMs): robust, solution-processable, organic nanoporous materials. *Chemical Communications*, 230-231 (2004).

12 Ghanem, B. S., McKeown, N. B., Budd, P. M., Selbie, J. D. & Fritsch, D. High‐performance membranes from polyimides with intrinsic microporosity. *Advanced Materials* **20**, 2766-2771 (2008).

13 Kim, S. & Lee, Y. M. Rigid and microporous polymers for gas separation membranes. *Progress in Polymer Science* **43**, 1-32 (2015).

14 Park, H. B., Han, S. H., Jung, C. H., Lee, Y. M. & Hill, A. J. Thermally rearranged (TR) polymer membranes for CO 2 separation. *Journal of Membrane Science* **359**, 11-24 (2010).

15 Song, Q. *et al.* Photo-oxidative enhancement of polymeric molecular sieve membranes. *Nature communications* **4**, 1918 (2013).

16 Du, N., Dal-Cin, M. M., Robertson, G. P. & Guiver, M. D. Decarboxylation-induced cross-linking of Polymers of Intrinsic Microporosity (Pims) for membrane gas separation†. *Macromolecules* **45**, 5134-5139 (2012).

17 Jones, C. W. & Koros, W. J. Carbon molecular sieve gas separation membranes-I. Preparation and characterization based on polyimide precursors. *Carbon* **32**, 1419-1425 (1994).

18 Chung, T.-S., Jiang, L. Y., Li, Y. & Kulprathipanja, S. Mixed matrix membranes (MMMs) comprising organic polymers with dispersed inorganic fillers for gas separation. *Progress in Polymer Science* **32**, 483-507 (2007).
19 Rezakazemi, M., Amooghin, A. E., Montazer-Rahmati, M. M., Ismail, A. F. & Matsuura, T. State-of-the-art membrane based CO 2 separation using mixed matrix membranes (MMMs): an overview on current status and future directions. *Progress in Polymer Science* **39**, 817-861 (2014).
20 Seoane, B. *et al.* Metal–organic framework based mixed matrix membranes: a solution for highly efficient CO 2 capture? *Chemical Society Reviews* **44**, 2421-2454 (2015).
21 Rangnekar, N., Mittal, N., Elyassi, B., Caro, J. & Tsapatsis, M. Zeolite membranes–a review and comparison with MOFs. *Chemical Society Reviews* **44**, 7128-7154 (2015).
22 Cavka, J. H. *et al.* A new zirconium inorganic building brick forming metal organic frameworks with exceptional stability. *Journal of the American Chemical Society* **130**, 13850-13851 (2008).
23 Tsuruoka, T. *et al.* Nanoporous nanorods fabricated by coordination modulation and oriented attachment growth. *Angewandte Chemie International Edition* **48**, 4739-4743 (2009).
24 Budd, P. M. *et al.* Solution‐processed, organophilic membrane derived from a polymer of intrinsic microporosity. *Advanced Materials* **16**, 456-459 (2004).
25 Schaate, A. *et al.* Modulated Synthesis of Zr‐Based Metal‐Organic Frameworks: From Nano to Single Crystals. *Chemistry‐A European Journal* **17**, 6643-6651 (2011).
26 Kandiah, M. *et al.* Synthesis and stability of tagged UiO-66 Zr-MOFs. *Chemistry of Materials* **22**, 6632-6640 (2010).
27 Rappé, A. K., Casewit, C. J., Colwell, K., Goddard Iii, W. & Skiff, W. UFF, a full periodic table force field for molecular mechanics and molecular dynamics simulations. *Journal of the American chemical society* **114**, 10024-10035 (1992).
28 Rappe, A. K. & Goddard III, W. A. Charge equilibration for molecular dynamics simulations. *The Journal of Physical Chemistry* **95**, 3358-3363 (1991).
29 Øien, S. *et al.* Detailed Structure Analysis of Atomic Positions and Defects in Zirconium Metal–Organic Frameworks. *Crystal Growth & Design* **14**, 5370-5372 (2014).
30 Semino, R., Ramsahye, N. A., Ghoufi, A. & Maurin, G. Microscopic model of the MOF/Polymer interface: a first step towards understanding the compatibility in Mixed Matrix Membranes. *ACS applied materials & interfaces* **8**, 809-819 (2016).
31 Mahajan, R. & Koros, W. J. Mixed matrix membrane materials with glassy polymers. Part 1. *Polymer Engineering & Science* **42**, 1420-1431 (2002).
32 Li, Y., Chung, T.-S., Cao, C. & Kulprathipanja, S. The effects of polymer chain rigidification, zeolite pore size and pore blockage on polyethersulfone (PES)-zeolite A mixed matrix membranes. *Journal of Membrane Science* **260**, 45-55 (2005).
33 Vu, D. Q., Koros, W. J. & Miller, S. J. Mixed matrix membranes using carbon molecular sieves: II. Modeling permeation behavior. *Journal of Membrane Science* **211**, 335-348 (2003).
34 Ren, H., Jin, J., Hu, J. & Liu, H. Affinity between metal–organic frameworks and polyimides in asymmetric mixed matrix membranes for gas separations. *Industrial & Engineering Chemistry Research* **51**, 10156-10164 (2012).
35 Goh, P. S., Ismail, A. F., Sanip, S. M., Ng, B. C. & Aziz, M. Recent advances of inorganic fillers in mixed matrix membrane for gas separation. *Separation and Purification Technology* **81**, 243-264 (2011).
36 Nik, O. G., Chen, X. Y. & Kaliaguine, S. Functionalized metal organic framework-polyimide mixed matrix membranes for CO 2/CH 4 separation. *Journal of Membrane Science* **413**, 48-61 (2012).
37 Anjum, M. W. *et al.* Modulated UiO-66-Based Mixed-Matrix Membranes for CO2 Separation. *ACS applied materials & interfaces* **7**, 25193-25201 (2015).

38 Rodenas, T. *et al.* Metal–organic framework nanosheets in polymer composite materials for gas separation. *Nature materials* **14**, 48-55 (2015).
39 Lau, C. H. *et al.* Ending aging in super glassy polymer membranes. *Angewandte Chemie International Edition* **53**, 5322-5326 (2014).
40 Lau, C. H. *et al.* Ending aging in super glassy polymer membranes. *Angewandte Chemie* **126**, 5426-5430 (2014).
41 Harms, S. *et al.* Aging and free volume in a polymer of intrinsic microporosity (PIM-1). *The Journal of Adhesion* **88**, 608-619 (2012).
42 Tiwari, R. R., Smith, Z. P., Lin, H., Freeman, B. & Paul, D. Gas permeation in thin films of "high free-volume" glassy perfluoropolymers: Part I. Physical aging. *Polymer* **55**, 5788-5800 (2014).
43 Brunauer, S., Emmett, P. H. & Teller, E. Adsorption of gases in multimolecular layers. *Journal of the American chemical society* **60**, 309-319 (1938).

Acknowledgements
H.H. thanks JST-PRESTO (JPMJPR141B) and City University of Hong Kong for financial support. E.S gratefully acknowledge JST-PRESTO (JPMJPR1417) and the Japanese Ministry of Environment as part of the project "Low Carbon Technology Research, Development and Demonstration Program". iCeMS is supported by World Premier International Research Initiative (WPI), MEXT, Japan.

Author contributions
B.G. conceived and designed the research. K.S., Y.K, synthesized and analysed PIM-1 MMMs, K.W. synthesized and analysed PEBAX MMMs, A.P. synthesized and analysed polyurethane MMMs, S.F. and S.K. evaluated MOF related data, Q.S. evaluated mixed membrane data, K.D. and H.H. performed simulations and H.K, S.K, E.S. supervised researchers in the project. All authors discussed the results and commented on the manuscript at all stages.

Additional information
Supplementary information is available in the online version of the paper. Reprints and permissions information is available online at www.nature.com/reprints. Correspondence and requests for materials should be addressed to E.S.

Competing financial interests
The results of this publication have been submitted for a patent filing application.

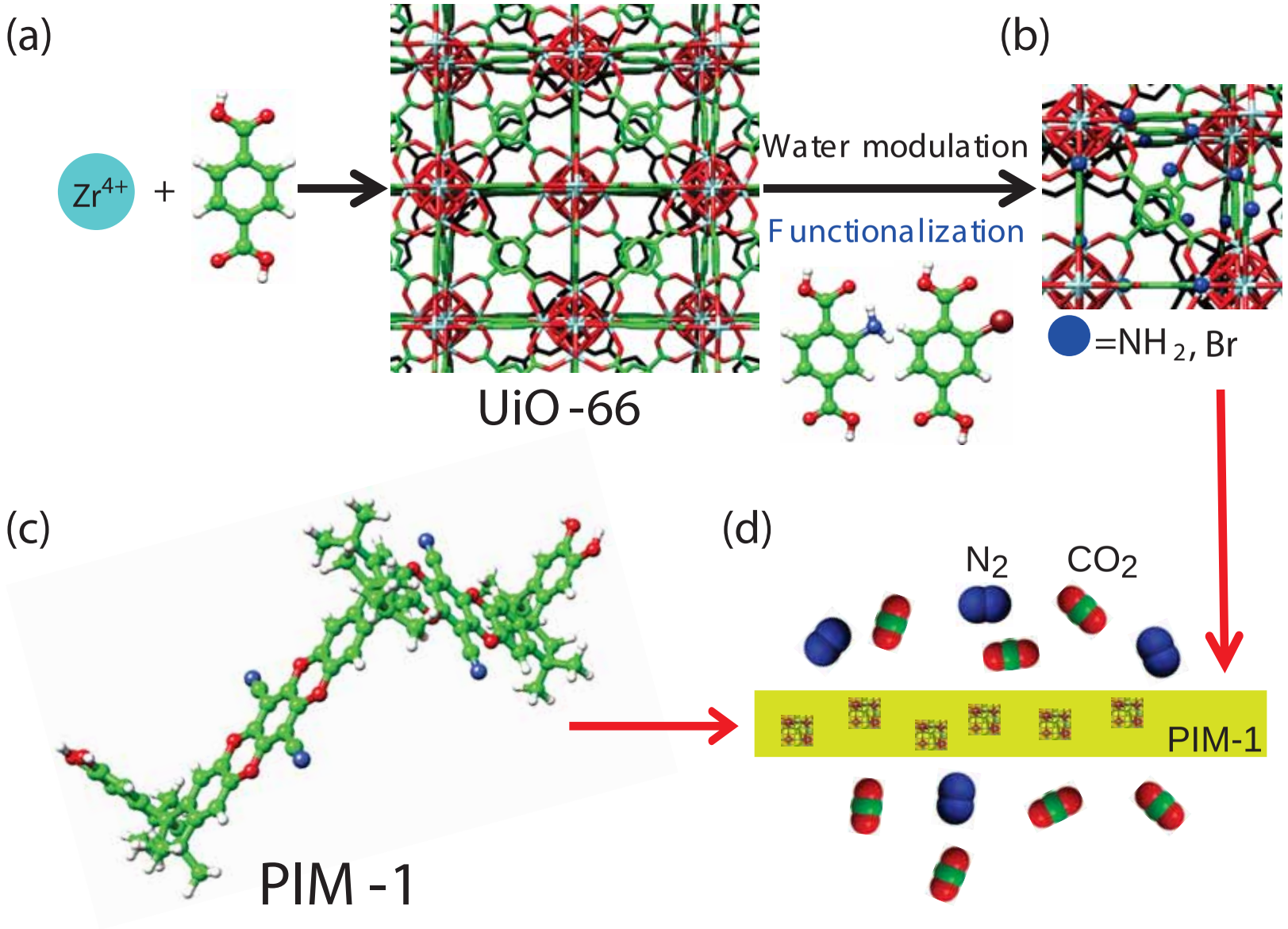
(a)
Zr^{4+}
+
UiO -66
Water modulation
Functionalization
(b)
=NH_2, Br
(c)
PIM -1
(d)
N_2
CO_2
PIM-1

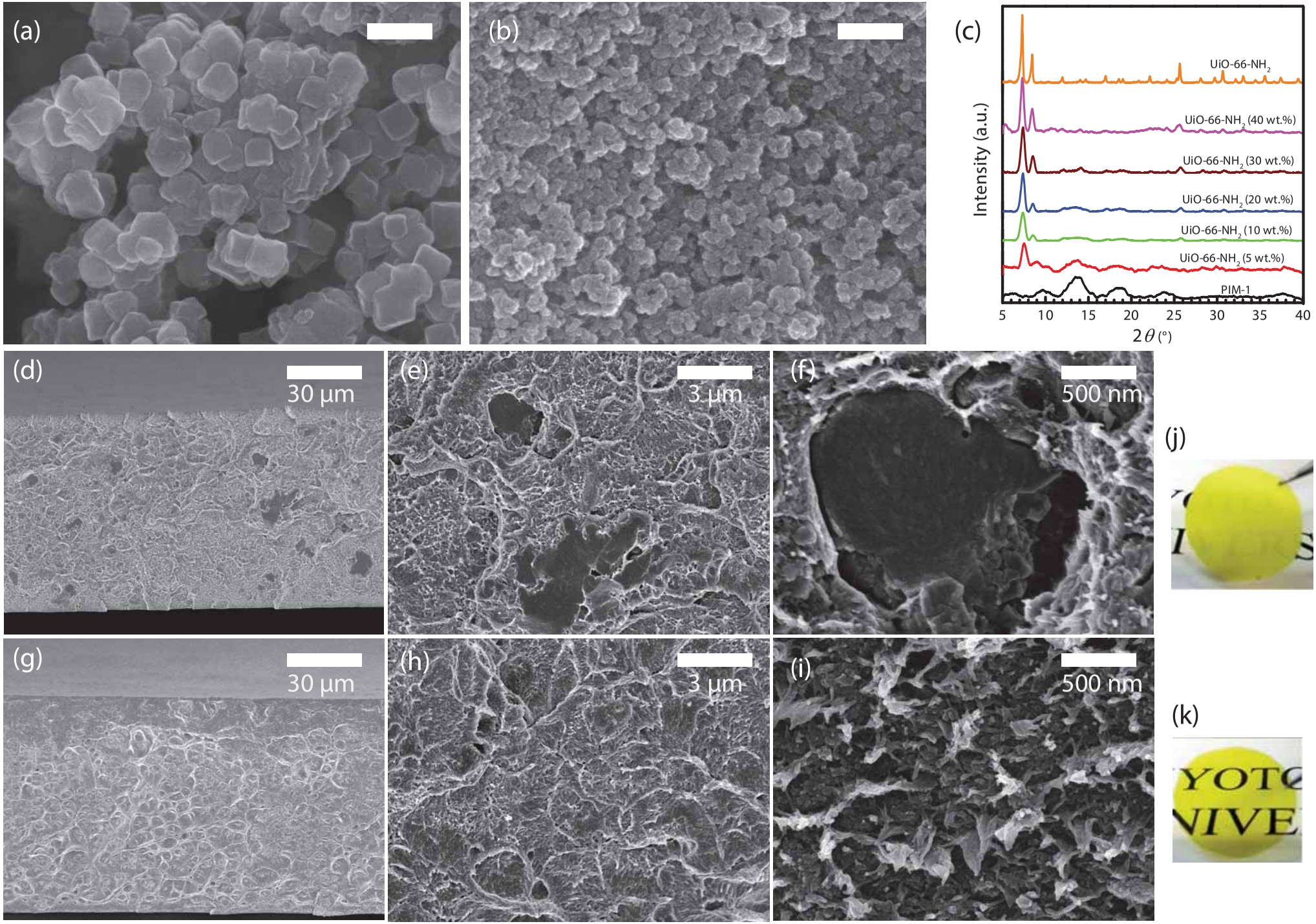
(a)
(b)
(c)
UiO-66-NH2
UiO-66-NH2 (40 wt.%)
UiO-66-NH2 (30 wt.%)
UiO-66-NH2 (20 wt.%)
UiO-66-NH2 (10 wt.%)
UiO-66-NH2 (5 wt.%)
PIM-1
Intensity (a.u.)
5 10 15 20 25 30 35 40
2θ (°)
(d)
30 µm
(e)
3 µm
(f)
500 nm
(g)
30 µm
(h)
3 µm
(i)
500 nm
(j)
(k)

(a) Models of UiO-66 and UiO-66-NH $_2$ frame works

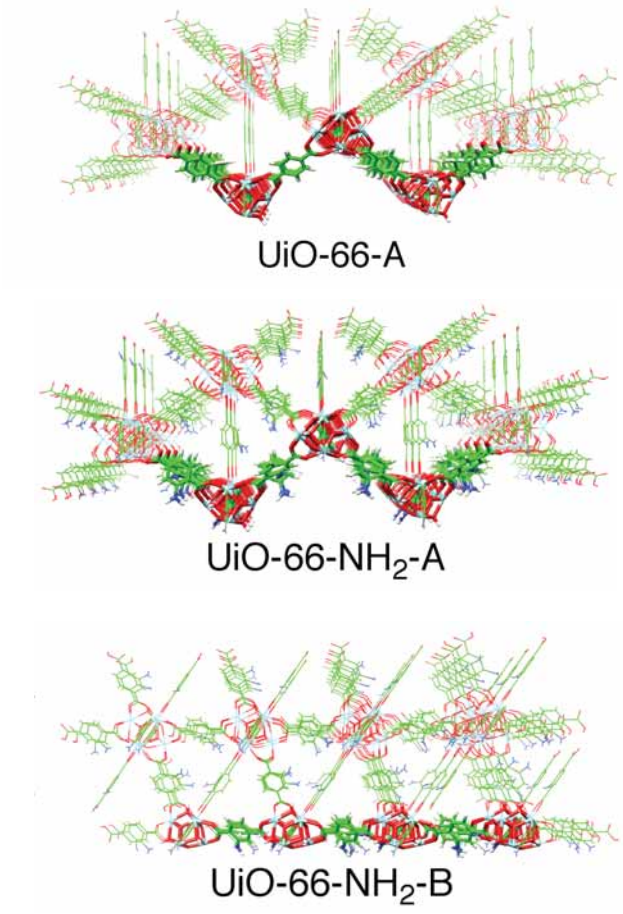

(b) UiO-66-A-1

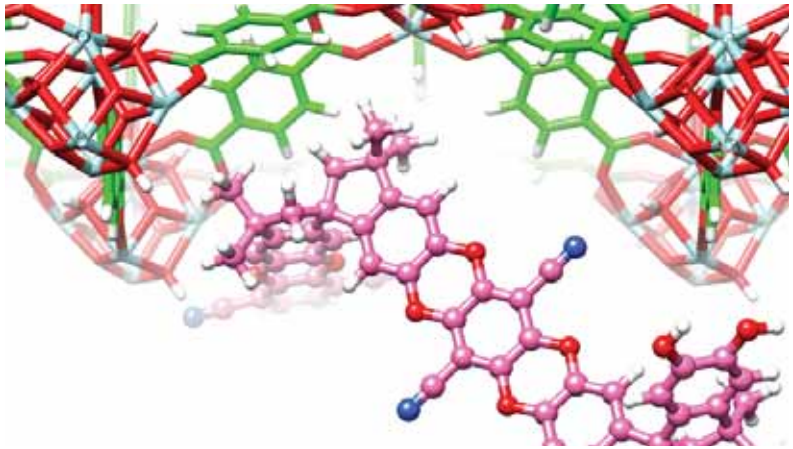

(c) UiO-66-NH $_2$-A-1

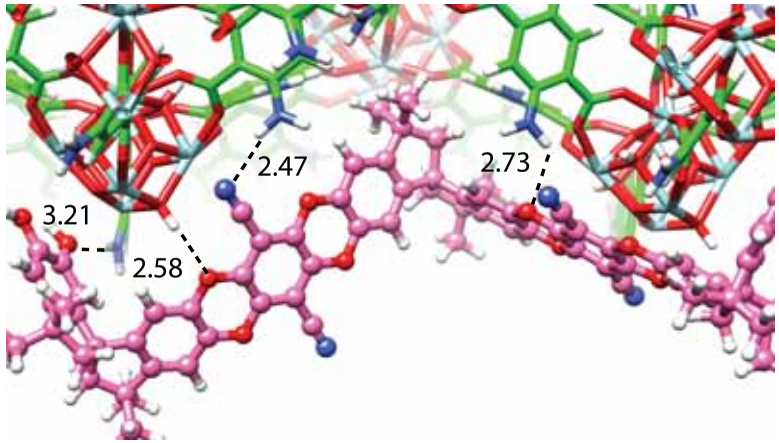

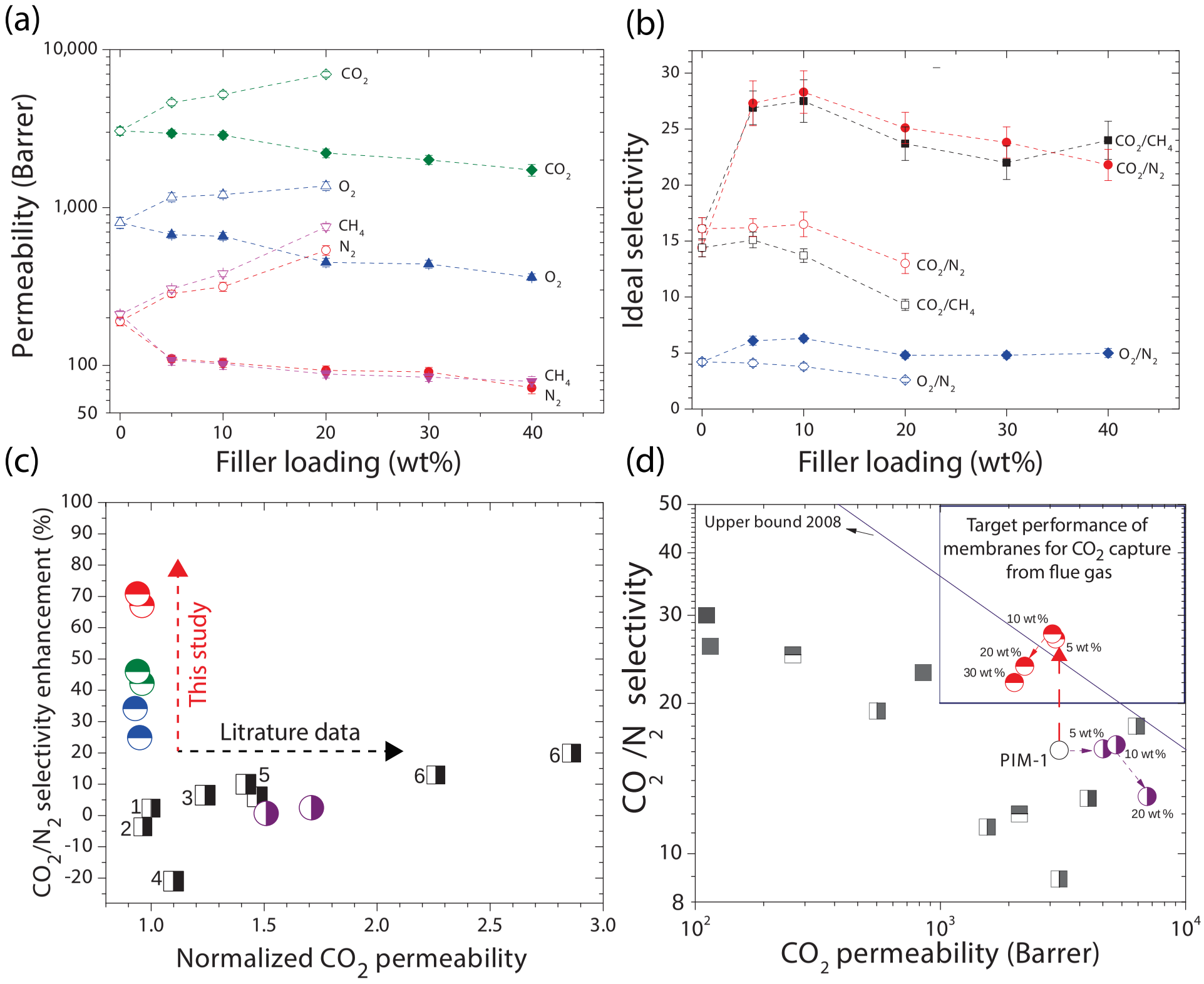
(a)
Permeability (Barrer)
10,000
1,000
100
50
CO2
CO2
O2
CH4
N2
O2
CH4
N2
0
10
20
30
40
Filler loading (wt%)
(b)
Ideal selectivity
30
25
20
15
10
5
0
CO2/CH4
CO2/N2
CO2/N2
CO2/CH4
O2/N2
O2/N2
0
10
20
30
40
Filler loading (wt%)
(c)
CO2/N2 selectivity enhancement (%)
100
90
80
70
60
50
40
30
20
10
0
-10
-20
This study
Litrature data
1
2
3
4
5
6
6
1.0
1.5
2.0
2.5
3.0
Normalized CO2 permeability
(d)
CO2 /N2 selectivity
50
40
30
20
10
8
Upper bound 2008
Target performance of membranes for CO2 capture from flue gas
10 wt %
5 wt %
20 wt %
30 wt %
5 wt %
PIM-1
10 wt %
20 wt %
10^2
10^3
10^4
CO2 permeability (Barrer)

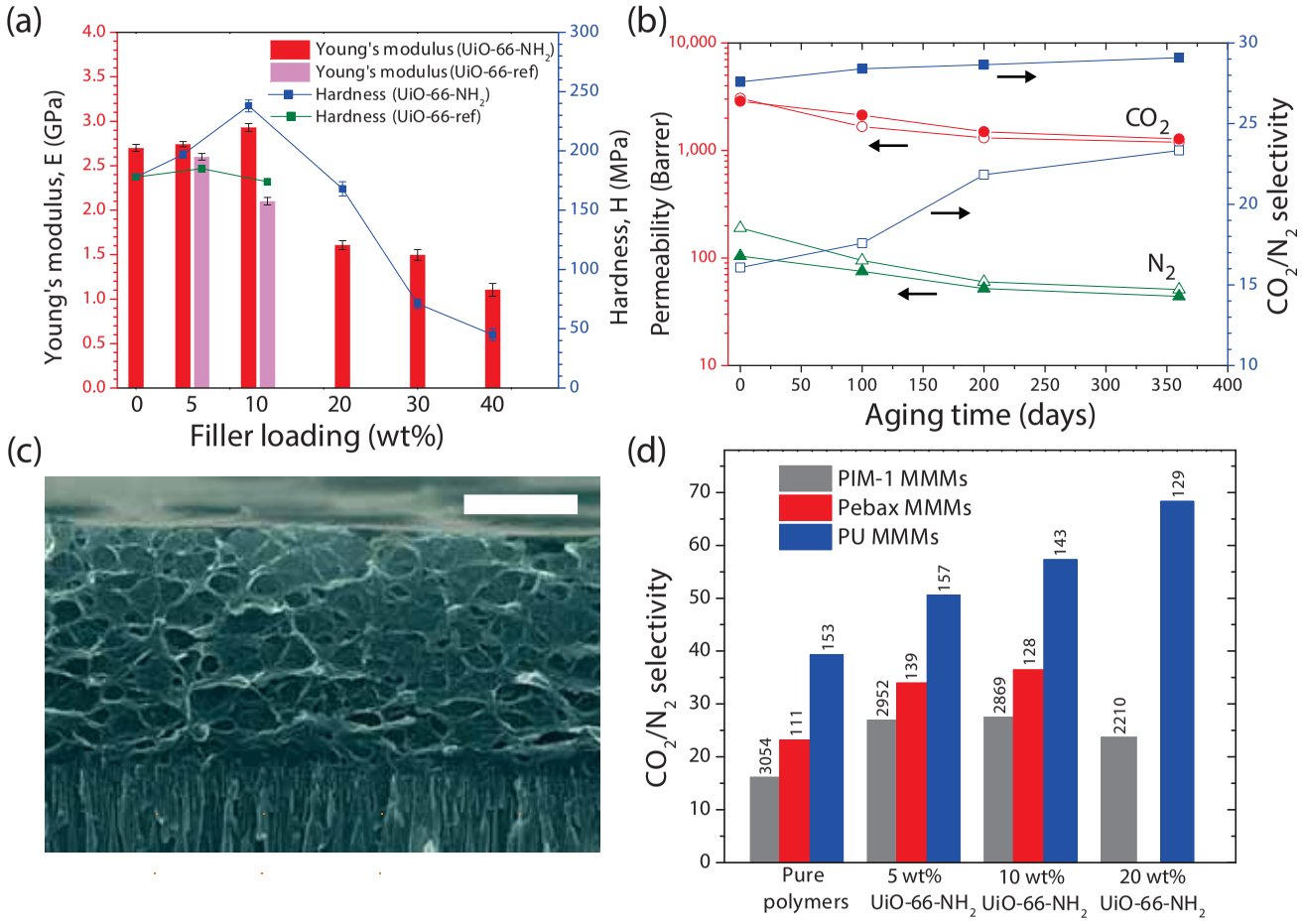
(a)
Young's modulus (UiO-66-NH2)
Young's modulus (UiO-66-ref)
Hardness (UiO-66-NH2)
Hardness (UiO-66-ref)
Young's modulus, E (GPa)
Hardness, H (MPa)
Filler loading (wt%)
(b)
CO2
N2
Permeability (Barrer)
CO2/N2 selectivity
Aging time (days)
(c)
(d)
PIM-1 MMMs
Pebax MMMs
PU MMMs
CO2/N2 selectivity
3054
111
153
2952
139
157
2869
128
143
2210
129
Pure polymers
5 wt% UiO-66-NH2
10 wt% UiO-66-NH2
20 wt% UiO-66-NH2